JOURNAL OF MATERIALS SCIENCE 30 (1995) 2235–2247

Microfracture and material removal in scratching of alumina

HOCKIN H. K. XU*, S. JAHANMIR
National Institute of Standards and Technology, Gaithersburg, MD 20899, USA

A bonded-interface sectioning technique is used to examine subsurface damage modes and to identify mechanisms of material removal in repeated single-point scratching of alumina as a function of grain size, load, and number of passes. In the fine grain alumina, the lateral and median crack system is observed, together with intergranular microcracks and intragrain twin/slip bands distributed within the plastic zone. The distributed form of damage, namely twin/slip bands and intergranular microcracks, are also observed in the coarse grain alumina; but no evidence is found for well-defined median and lateral cracks in this material. The mechanism of material removal in alumina is identified as grain dislodgement resulting from grain boundary microcracking, irrespective of the grain size. Extension of lateral cracks is found to contribute to the material removal process only in the fine grain alumina scratched under a large load and after several passes. A model for the microfracture-controlled material removal process is proposed that relates the volume of material removed to the applied load and material properties including grain size, elastic modulus, hardness, and short-crack toughness. Removal rate is shown to be proportional to grain size $l^{1/2}$ and to load P^2. The model and the experimental results obtained in scratching are used to describe the action of an individual abrasive grit in grinding and other abrasive machining processes.

1. Introduction

The mechanisms of material removal in abrasive wear and grinding of ceramics have been described by analogy to the type of damage produced by indentation. In quasi-static indentation [1] and single-point scratch testing [2–6] of amorphous and fine grained ceramics, two types of cracks have been observed: median cracks that are normal to the surface, and subsurface lateral cracks that are parallel to the surface. While median cracks are generally associated with strength degradation in fracture tests [7], lateral cracks are assumed to be responsible for material removal [8–11]. Propagation of the lateral cracks along the two sides of the scratch has been proposed as the primary mechanism for fragmentation and material removal [8, 9]. Therefore, the total amount of material removed by abrasive wear and grinding has been related to the size of the lateral cracks that are produced beneath the scratch [8, 9]. With this assumption, Evans and Marshall [9] derived an expression that relates the volume of removed material with the normal load and material properties that determine the size of the lateral cracks:

$$V = \delta P^{9/8}(E/H)^{4/5}/(K_c^{1/2}H^{5/8}) \quad (1)$$

where V is the total volume of material removed per unit scratch length, P is the normal load, E is the Young's modulus, H is the hardness, K_c is the fracture toughness of the material, and δ is a material-independent constant. This equation, while providing important insights into the relationship between the material removal rate and the mechanical properties of the material, does not directly relate the removal rate with the microstructure, for example grain size of the material. The purpose of the present paper is, therefore, to elucidate the mechanisms of material removal in scratching of polycrystalline ceramics, with a particular emphasis on the effect of grain size.

Microstructure plays a significant role in controlling the mechanical properties and machinability of ceramics [12–17]. In alumina, for example, it has been shown that fracture toughness, measured in samples containing long cracks of the order of millimetres, increases as the grain size is increased; but for a crack size of the order of one grain size, the short-crack toughness decreases [18, 19]. Increasing the grain size of alumina also improves its machinability [12, 20, 21]. For example, at the same depth of cut, the normal grinding force of a coarse grain alumina is only one third of that of a fine grain alumina [20]. These results suggest that microstructure, and particularly the grain size, has a significant influence on the material removal process in machining. Therefore, models for machining of ceramics must consider the

* Guest scientist, from Department of Mechnical Engineering, University of Maryland, College Park, MD 20742, USA

0022–2461

role of microstructure in addition to the influence of lateral cracks that may form beneath the surface.

A necessary condition for the lateral-cracking mechanism to be effective in abrasive machining of ceramics is that such subsurface cracks exist. Formation of lateral cracks in glasses, single crystal ceramics, and fine grain polycrystalline ceramics has been confirmed in indentation and scratch tests [1–6]. However, the material removal process in grinding has not been clearly shown to be related to the propagation of lateral cracks, especially for polycrystalline ceramics. Furthermore, in ceramics with a coarse microstructure and toughened ceramic composites with weak grain boundaries and interfaces, the crack formation process can be strongly influenced by the microstructure. This was recently demonstrated in Hertzian indentation tests by Lawn and coworkers [22–26]. While the subsurface Hertzian indentation damage of a fine grain alumina showed classical cone fracture, that of a coarse grain alumina showed an entirely different damage pattern. Instead of cone cracks, the subsurface zone consisted of distributed damage in the form of intragrain twin/slip bands and intergranular microcracks [22, 23]. The influence of microstructure on the transition from cone-cracking to distributed damage was also observed in mica-containing glass ceramics [24], silicon carbide [25] and silicon nitride [26].

Direct observation of subsurface damage in scratching and grinding is critical in the investigation of the material removal process, because this can provide key information on the mechanisms of material removal. Conventional sectioning techniques involving cutting and polishing may remove the damage patterns of interest and produce additional damage and artifacts. Recently, a bonded-interface sectioning technique was proposed for the direct observation of subsurface damage in Hertzian contacts [22, 24–26]. This technique has been effectively applied to grinding of a coarse grain alumina to identify the subsurface grinding damage [27]. It was found that grinding damage in this material primarily consists of intergranular and transgranular microcracks and intragrain twin/slip bands [27]. No evidence was found for the presence of well-defined median and lateral cracks.

The bonded-interface sectioning technique is used in the present study to examine the subsurface damage modes and to identify the mechanisms of material removal in repeated single-point scratching of alumina ceramics with different grain sizes. The mechanisms of material removal in scratching is discussed in the light of the observed surface and subsurface damage modes, and a microfracture model is proposed for the material removal process. This model, which is based on material removal by grain dislodgement rather than propagation of lateral cracks, relates the volume of material removed to the load, grain size and number of passes in repeated scratching. The experimental results and the model are then used to describe the action of an individual abrasive grit in grinding and other abrasive machining processes.

2. Experimental procedure

2.1. Materials and specimen preparation

Polycrystalline alumina samples prepared and characterized by Chantikul *et al.* [18] for an earlier study on the relationship between grain size and toughness were used in the present investigation. In their work, an ultra-high-purity alumina powder was doped with a small amount of MgO (Mg/Al = 500 at. p.p.m.) and was prepared for sintering in a class A-100 clean room [18]. The green compacts were pressureless-sintered at 1550 °C for 30 min to produce specimens with a density > 99% of the theoretical value and a grain size of 1.8 μm [18]. The specimens were then heat-treated at prescribed hold times and temperatures to obtain a uniform and equiaxed grain structure of various sizes [18]. The average grain size of specimens selected for use in the present study were 3, 21 and 35 μm with a narrow grain size distribution and a small intrinsic flaw population predominantly consisting of small pores at the grain boundary triple-point junctions. The toughness curves of these aluminas, as characterized earlier by Chantikul *et al.* [18], are shown in Fig. 1. The toughness values were calculated from strength measurements performed in biaxial fracture tests on samples indented at various loads to produce a wide range of indentation crack sizes. As shown in Fig. 1, the long-crack toughness values for the aluminas used in the present investigation are 3.0, 4.0 and 4.8 MPa $m^{1/2}$ at grain sizes of 3, 21 and 35 μm, respectively. The short-crack toughness of these aluminas, however, depends on the crack size. For example for a crack size equivalent to the grain size, the toughness decreases as the grain size is increased. This is opposite to the effect of grain size on the long-crack toughness. The indentation hardness of these aluminas range from 20–25 GPa, and are not very sensitive to the grain size [28].

The specimens were machined into bars with dimensions of 2.5 × 2.5 × 20 mm. One rectangular surface of each specimen was polished consecutively with 30, 15, 6, 3 and 1 μm diamond paste. The bonded-interface sectioning technique, as described previously

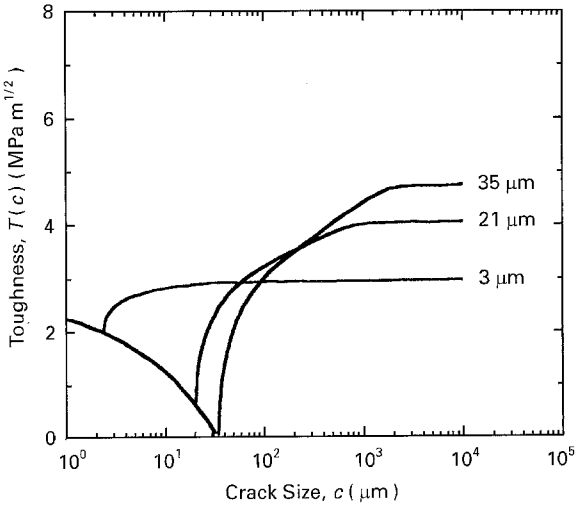

Figure 1 Toughness versus crack size for the three alumina ceramics used in the present investigation. The grain size of each alumina is indicated on the figure. (Adapted from Ref. 18).

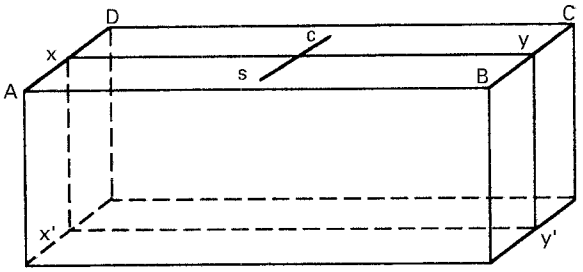

Figure 2 Schematic of the bonded-interface sectioning technique. The polished surfaces of two specimens were bonded together at the interface xyx'y'. A scratch was made on the top surface ABCD shown by the line "sc".

[27], was used to reveal the subsurface scratch damage. The polished rectangular surfaces of two specimens of each grain size were bonded face-to-face with "super-glue". Clamping pressure was applied during bonding to ensure a narrow interface (approximately 1 μm thick) in order to avoid artificial damage at the interface during scratching. Fig. 2 schematically shows the two specimens bonded together at the xyx'y' interface of the two polished surfaces. The upper surface ABCD was then ground to obtain a flat surface and was polished to remove the grinding damage. The polishing procedure was the same as that used for the rectangular faces.

2.2. Scratching and damage evaluation

Scratches were made with a diamond conical indentor having an apex angle of 120° and a spherical tip radius of about 10 μm. Each scratch was made with the indentor oriented normal to the plane ABCD and moving perpendicularly across the interface line xy, as shown by the line "sc" in Fig. 2. Testing was performed under a constant load in laboratory air with a relative humidity of 40–50%. Normal loads of 10, 20, 30 and 40 N were used in making the scratches. The load was applied with a universal testing machine. The bonded specimens were attached to a micrometer stage and scratching was carried out by manually moving a micrometer manipulator at an approximate sliding speed of 0.5 mm s^{-1}. The scratch length was approximately 3 mm and was located symmetrically across the bonded interface. Both single-pass and unidirectional multiple passes up to 20 were made.

After scratching, the two specimens were separated by melting the glue on a hot-plate. The specimens were then cleaned with acetone and alcohol. The polished surfaces were coated with gold and viewed in an optical microscope using Nomarski interference illumination and in a scanning electron microscope (SEM). In order to remove the loosely attached debris, the specimens were cleaned in an ultrasonic bath containing acetone for 5 min. To determine the amount of material removed in scratching, the scratch profiles were then measured by surface profilometry. A total of five profiles were taken across each scratch. These profiles were used to estimate the average cross-sectional area of the scratches.

3. Experimental results

3.1. Material removal process

The scratches produced in the fine grain alumina (3 μm grain size) at a normal load of 20 N are shown in the optical micrographs with Nomarski illumination in Fig. 3 for the number of passes $n = 1$, 2, 5 and 10. These micrographs clearly show that the width of the scratches remains constant as the number of passes are increased. However, the appearance of the areas inside the scratches are different, suggesting increased surface damage with repeated scratching. This difference can be clearly seen in the SEM micrographs in Fig. 4 obtained from the central regions of the scratches. A significant contact damage in the form of intergranular microcracks, pointed by the arrows, is shown in Fig. 4(a) after one pass. These intergranular microcracks eventually result in grain dislodgement

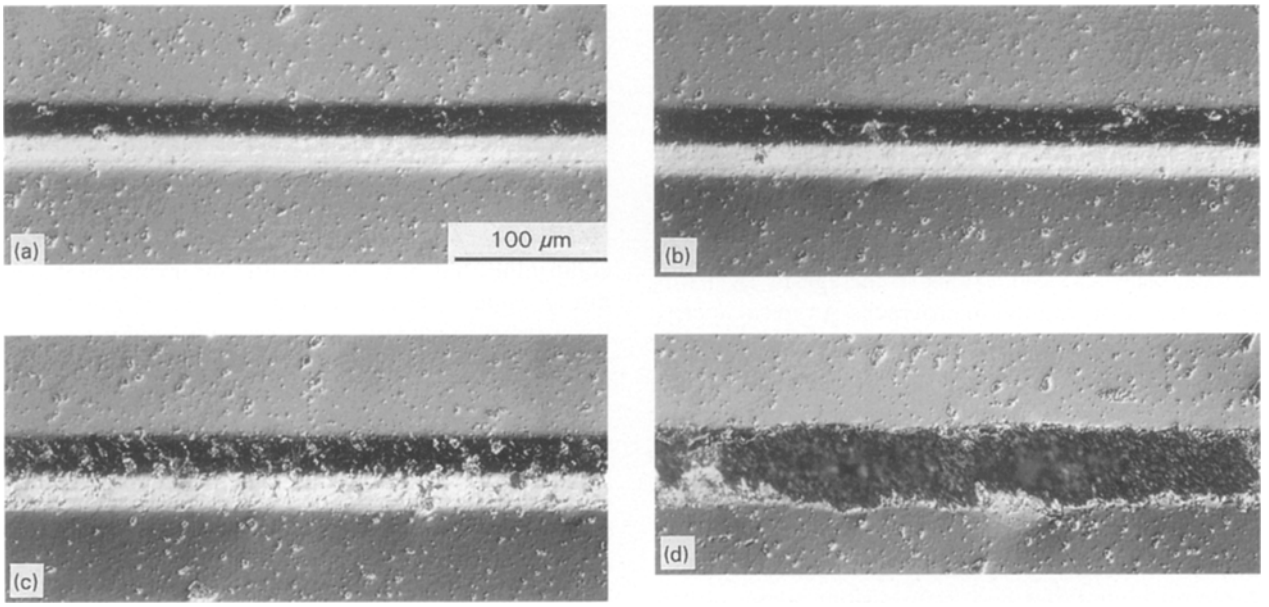

Figure 3 Optical micrographs with Nomarski interference illumination of scratches produced in the fine grain alumina (grain size = 3 μm), at a load $P = 20$ N for different number of passes: (a) $n = 1$, (b) $n = 2$, (c) $n = 5$ and (d) $n = 10$.

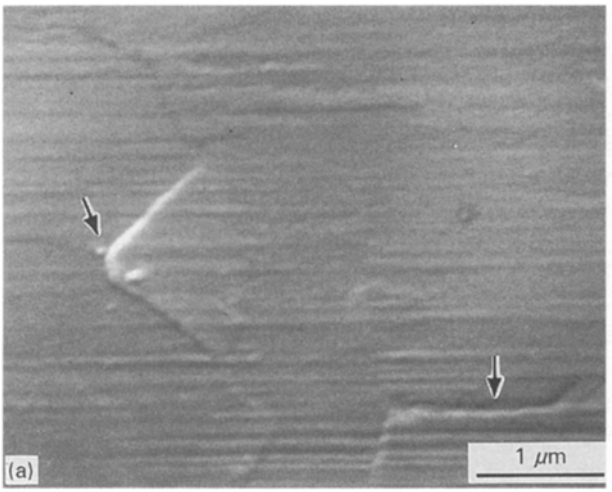

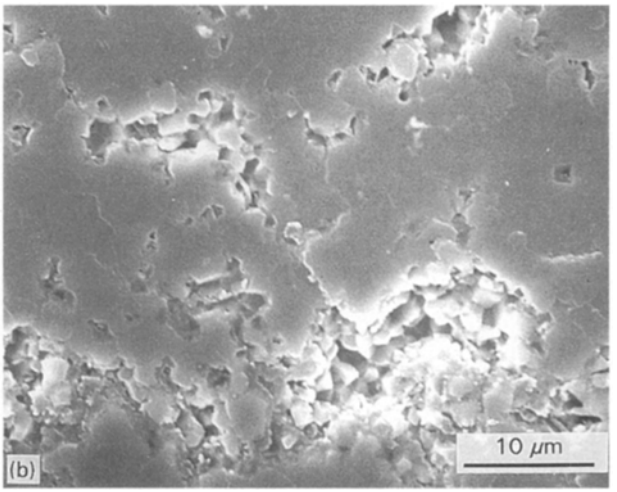

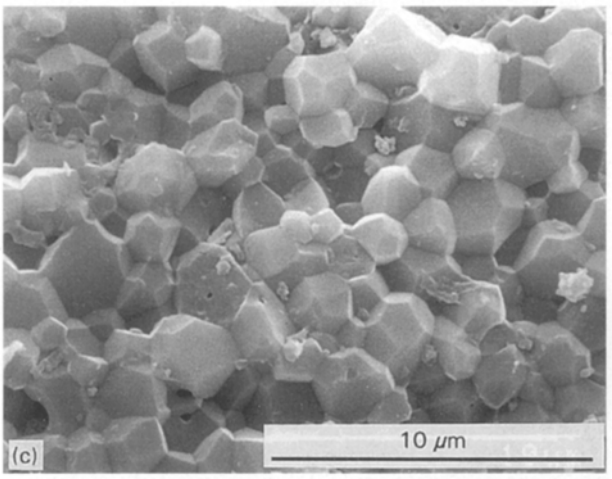

Figure 4 SEM micrographs of the scratches shown in Fig. 3: (a) $n = 1$, arrows point at grain boundary microcracks; (b) $n = 5$, note that material has been removed by intergranular fracture; and (c) $n = 10$, note the grain structure of the alumina, suggesting intergranular fracture and grain dislodgement as the primary material removal mechanism.

and material removal after repeated scratching, as shown by the SEM micrographs in Figs 4(b) and (c) after 5 and 10 passes, respectively. It is important to note that examination of the scratches near the bonded interface revealed little or no superfluous damage due the interface.

The subsurface scratch damage in the fine grain alumina revealed by the bonded-interface sectioning technique is shown in the optical micrographs with Nomarski illumination in Fig. 5 for the number of passes $n = 1$, 5 and 10. Median and lateral cracks (denoted as "m" and "l") extending from the plastic zone beneath the contact area are visible in the optical micrographs. SEM examination of the plastically deformed zone revealed extensive intragrain twin/slip bands and intergranular microcracks. A typical micrograph, taken near the area indicated by the arrow in Fig. 5(a), is shown in Fig. 6. Although after 5 and 10 passes, a substantial amount of material has been removed from the plastic zone (Figs 5(b) and (c)), the median and lateral cracks are still visible and have not propagated to cause material removal. In fine grain aluminas scratched under a 20 N load, therefore, material is removed by propagation of microcracks along the grain boundaries and grain dislodgement, rather than by the extension of lateral cracks toward the surface.

3.2. Effect of grain size

A dramatic increase in the extent of surface damage is observed in the coarse grain alumina (35 μm) as compared with that in the fine grain counterpart. This is shown by the optical micrographs in Fig. 7 for a load of 20 N after 1, 2 and 5 passes. Extensive intragrain twin/slip bands and microcracks are visible, so are the pits from grain dislodgement as indicated by the arrows. Corresponding SEM micrographs are shown in Fig. 8, where it is evident that material removal primarily occurs by dislodgement of grains resulting from integranular microcracks. The small debris observed in Fig. 8(c) are likely a result of chipping microfracture within the grains and/or entrapment and fracture of the dislodged grains between the indentor and the alumina surface.

The section views of the scratches in the coarse grain alumina reveal a radical departure from the classical median/lateral cracking patterns seen in the fine grain alumina. As shown in Fig. 9, the subsurface damage beneath the scratches in the coarse grain alumina consists of twin/slip bands and intergranular microcracks. Well-defined median and lateral cracks, such as those observed in Fig. 5 for the fine grain alumina, are not evident in the coarse grain material, confirming that also in this alumina propagation of intergranular microcracks and grain dislodgement are the primary steps for the material removal process.

3.3. Effect of Scratch Load

Increasing the normal load in scratching significantly increases the size of the scratch impressions and the level of subsurface damage. The scratches performed on the fine grain alumina under a normal load of 40 N after 1, 5 and 10 passes are shown in the optical micrographs in Fig. 10. SEM examination showed that, similar to the observations made for the

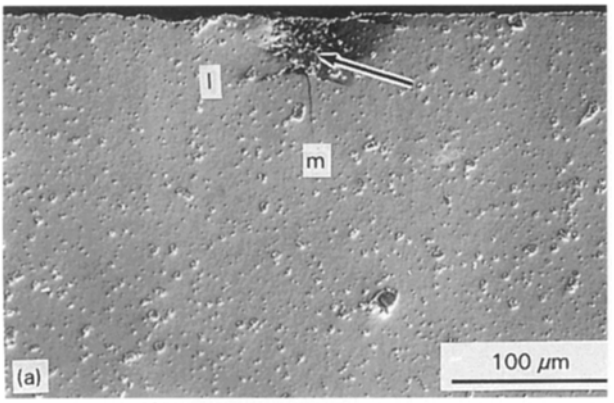

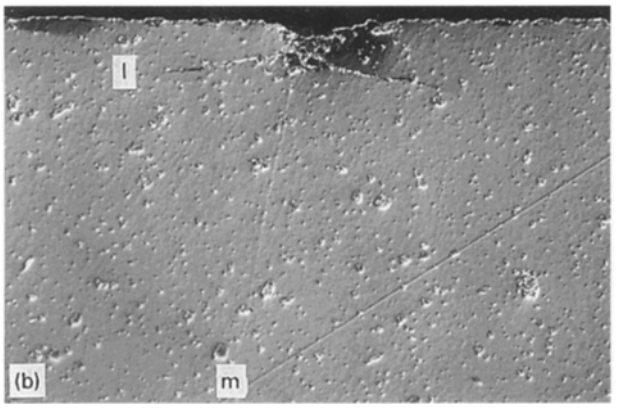

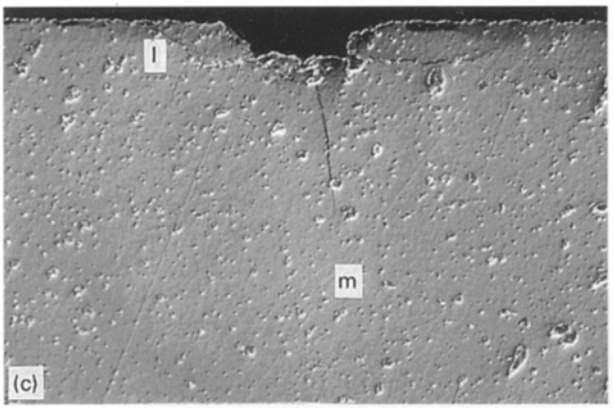

Figure 5 Optical micrographs with Nomarski illumination of section views for the fine grain alumina, showing subsurface scratch damage at $P = 20$ N after different passes: (a) $n = 1$, (b) $n = 5$, and (c) $n = 10$; "l" and "m" denote lateral and median cracks, respectively. Note the increase in the amount of material removed as the number of passes is increased. Also note that material is mainly removed from within the plastic zone.

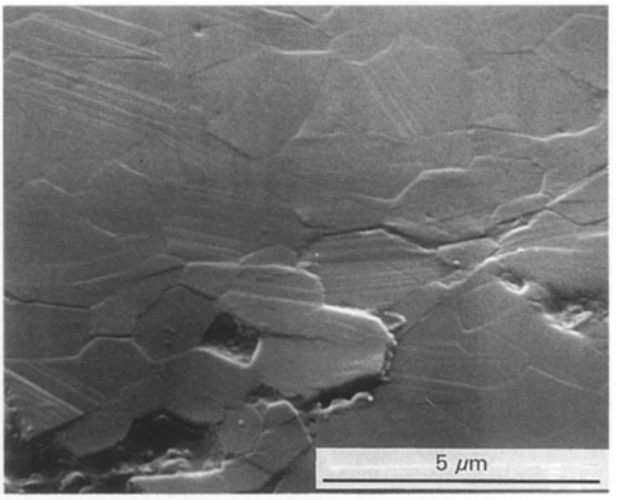

Figure 6 High magnification SEM view of the area within the plastic zone indicated by the arrow in Fig. 5(a). Note extensive intergranular microcracks and intragrain twin/slip bands.

20 N-load, material is removed by intergranular microcracking and grain dislodgement after 5 passes. Some material, however, has been removed by lateral crack chipping after 10 passes (Fig. 10(c)), since the width of the scratch is much larger than the contact width in certain locations along the scratch. Examination of the repeated scratches made under a 40 N-load in this alumina revealed that the change in the removal mechanism from grain dislodgement to lateral crack chipping had occurred after 7 passes.

The corresponding subsurface damage patterns in the fine grain alumina scratched under a 40 N-load are shown in Fig. 11 after 1, 5 and 10 passes. The median and lateral cracks are longer than those observed at a load of 20 N. After 5 passes (Fig. 11(b)), material removal is still confined to the plastic zone. The size of the area removed after 10 passes is significantly larger than the size of the plastic zone, confirming that lateral crack chipping has contributed to the material removal process. Notice, however, that only a small portion of the material above the lateral cracks has been removed (Fig. 11(c)) and that the lateral cracks have not fully propagated to the surface.

The surface features for the coarse grain alumina scratched under a 40 N-load, are shown in Fig. 12 after 1, 2 and 5 passes. Extensive twin/slip bands and intergranular microcracks are again evident. The scratch width increases significantly with load. For example, the scratch width obtained under a load of 40 N after 5 passes is approximately twice as large as the scratch obtained under a load of 20 N. The corresponding subsurface damage pattern in the coarse grain material is shown in Fig. 13. The nature of the damage still takes the form of twin/slip bands and intergranular microcracks. It is important to note that even at this large load, no evidence is found in the coarse grain material for well-defined median/lateral cracks. Material is removed mainly by grain dislodgement, with some small-scale chipping within the individual grains.

3.4. Material removal volume

To quantitatively evaluate the effect of grain size and load on the volume of removed material, the scratch profiles were measured by surface profilometry. Examples of scratch profiles for the fine grain alumina under a load of 20 N are shown in Fig. 14 after 1 and 10 passes. Fig. 14(a) shows that after one pass, the scratch depth is less than 0.5 μm. It is also observed that the two sides of the scratch are raised, possibly by lateral crack up-lift [29]. However, after 10 passes (Fig. 14(b)) a substantial amount of material is

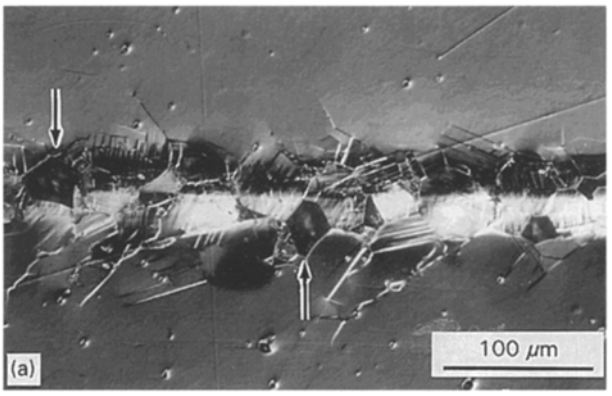

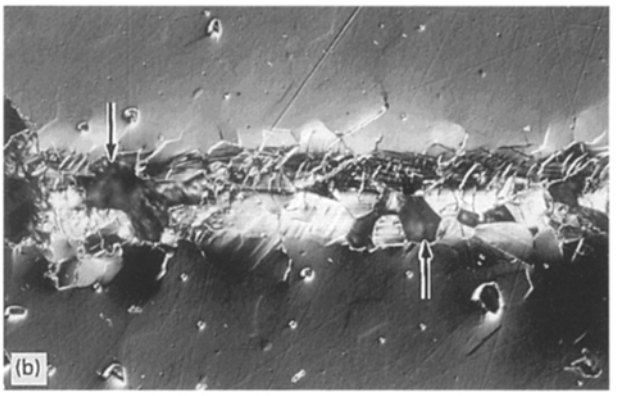

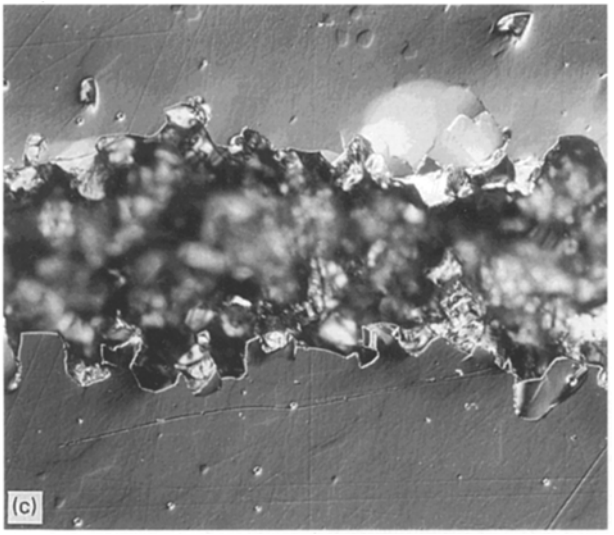

Figure 7 Optical micrographs with Nomarski illumination showing the scratches in the coarse grain alumina (grain size = 35 μm), at $P = 20$ N after different passes: (a) $n = 1$, (b) $n = 2$, and (c) $n = 5$. Arrows point to pits produced by grain dislodgement. Note extensive twin/slip bands and microcracks in (a) and (b).

removed and the scratch depth is nearly 7 μm. Using the scratch profiles, the average cross-sectional area of each scratch was calculated to estimate the total volume of material removed per unit scratch length, in units of $\mu m^3\ \mu m^{-1}$. In this calculation, the net cross-sectional area of the removed material was estimated by subtracting the area of the material raised above the surface reference line on the two sides of the scratches from the area below the reference line. The measured volume per unit scratch length is plotted in Fig. 15 as a function of grain size and load. Each data point is an average of five measurements at different positions along each scratch. The standard deviation of the measurements were typically about 30% of the average values.

As seen in Fig. 15, the removed volume is initially very small. However, it increases after a critical number of passes is reached, particularly at low loads and for the fine grain alumina. The critical number of passes for this transition depends on the grain size and load. For example, for the alumina with a grain size of 3 μm, scratched under a load of 20 N, 10 passes are required for the transition; whereas the transition occurs after 2 passes for the alumina with a grain size of 21 μm. After the transition, the removed volume increases almost linearly with the number of passes.

4. A model for microfracture-controlled material removal process

The results obtained for repeated scratching of alumina ceramics clearly show that the material removal process in scratching consists of formation and propagation of microcracks along the grain boundaries leading to grain dislodgement. Although a well-developed median/lateral crack system was observed for the fine grain alumina, this crack system did not play a major role in the removal process, except under high loads and after many repeated passes. Furthermore, this crack system was not observed in the coarse grain alumina. Therefore, a new microfracture model is needed to describe the effect of load and grain size on the material removal process in abrasive wear and grinding.

The proposed model is based on the original model by Cho *et al.* [30] and its modification by Liu and Fine [31]. Following the suggestion made by Cho *et al.* [30], we consider that microcracks initiate from initial grain boundary flaws as a result of loading. Using the equation proposed by Liu and Fine for wear [31], we then develop a fracture mechanics criterion to predict the onset of local microfracture (or crack propagation along the grain boundaries). The fracture model proposed by Fu and Evans [32] is then used to calculate the total fraction of microcracked grain boundary facets. This fraction is used to develop an equation for the volume of material removed by scratching. In the previous models, the grain boundary intrinsic toughness was estimated by assuming that spontaneous fracture occurs in alumina at a critical grain size. In our model, we incorporate the short-crack toughness of the material directly into the fracture criterion. Also, we include an estimate for the effect of applied load on the rate of damage accumulation and the local grain boundary stress.

The size of the initial flaws c_0 is assumed to scale with the grain size l; such that $c_0 = \beta l$, where β is a scaling coefficient [30, 33]. For the aluminas used in the present study, a value of 0.8 is suggested by Cho *et al.* [30] for the intrinsic grain boundary flaws from

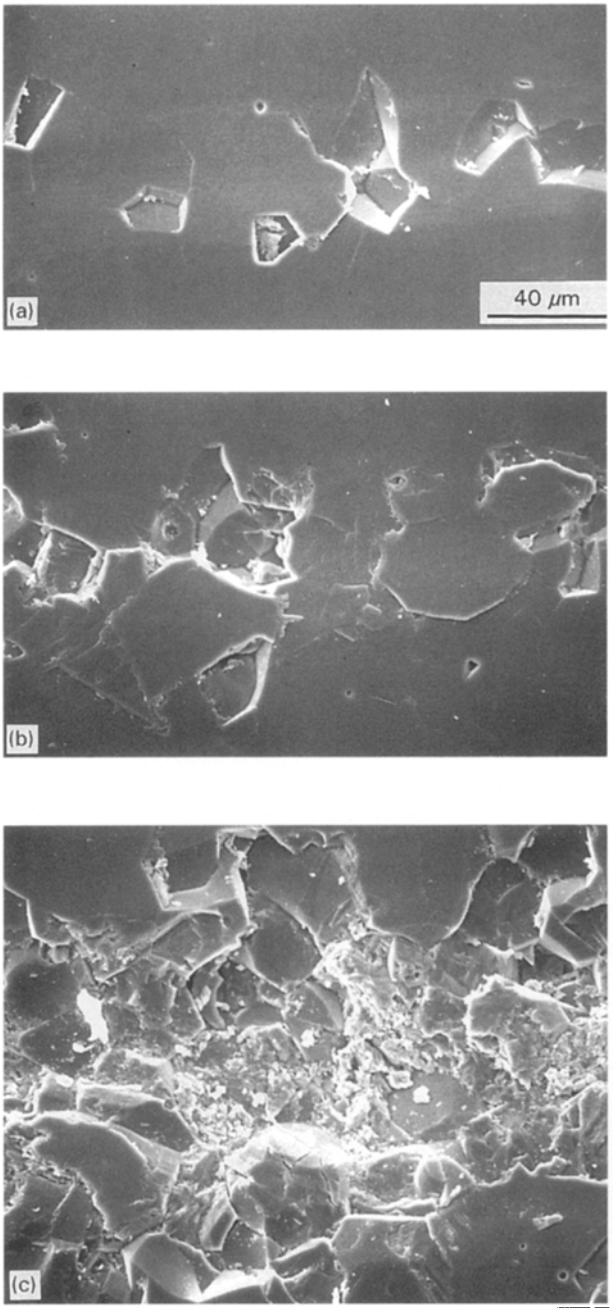

Figure 8 SEM micrographs of the scratches shown in Fig. 7 after different passes: (a) $n = 1$, (b) $n = 2$ and (c) $n = 5$. Scratch direction is horizontal. Note that material has been removed by grain dislodgement.

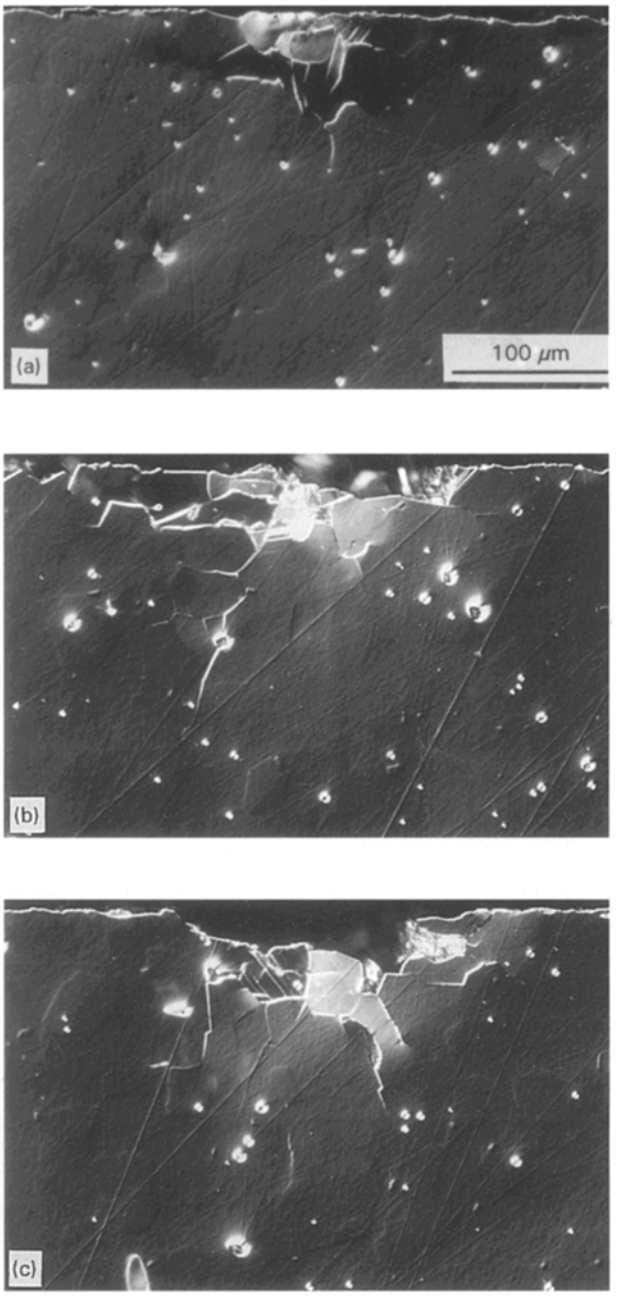

Figure 9 Optical micrographs showing subsurface damage in the coarse grain alumina, at $P = 20$ N after different passes: (a) $n = 1$, (b) $n = 2$ and (c) $n = 5$. Note the absence of well-defined lateral and median cracks. The subsurface scratch damage here takes the form of zigzag microcracks along the grain boundaries. Twin/slip bands as shown in Fig. 6 for the fine grain alumina are also present here.

which microcracks propagate during loading. The driving force for propagation of microcracks from such flaws is the local grain boundary tensile stress, which consists of the tensile stress σ_T due to the applied load in scratching, the tensile stress σ_D induced by damage accumulation (e.g. dislocation pile-up), and the intrinsic residual stress σ_I from thermal expansion anisotropy. The equilibrium condition for fracture at a grain boundary facet can be written as [31, 33]

$$K_T + K_D + K_I = T_0 \quad (2)$$

where K_T, K_D and K_I are the stress intensity factors associated with σ_T, σ_D and σ_I; and T_0 is the intrinsic grain boundary toughness.

Taking into consideration that fracture proceeds along the grain boundary facets with a tensile residual stress σ_I, the toughness T at these facets can be related to the intrinsic residual stress by [33]

$$T = T_0 - K_I \quad (3)$$

For materials with R-curve behaviour (see Fig. 1), the fracture toughness is a function of crack size c, i.e., $T = T(c)$. Since the initial crack size is assumed to be proportional to the grain size, i.e., $c = \beta l$, then the toughness T is also a function of grain size, i.e., $T = T(\beta l)$.

By substituting Equation 3 into Equation 2 and using the relationship between crack size and stress intensity factor, the equilibrium condition may be

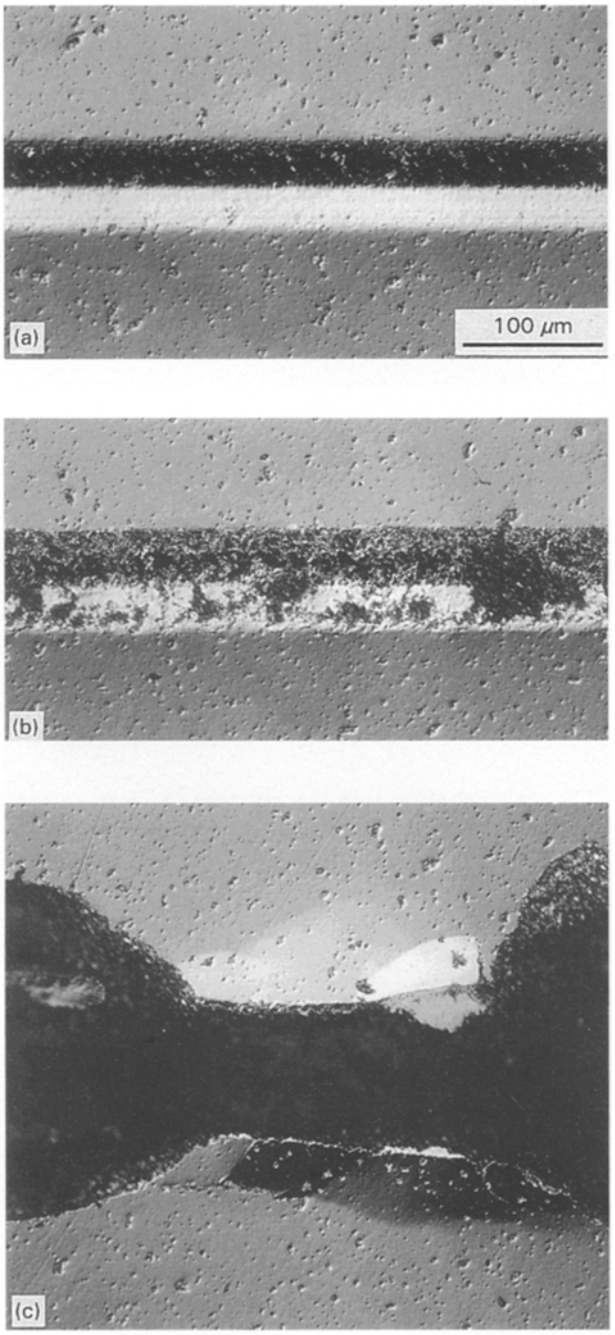

Figure 10 Optical micrographs with Nomarski illumination of the scratches in the fine grain alumina, at $P = 40$ N after different passes: (a) $n = 1$, (b) $n = 5$ and (c) $n = 10$. Note lateral crack chipping in (c).

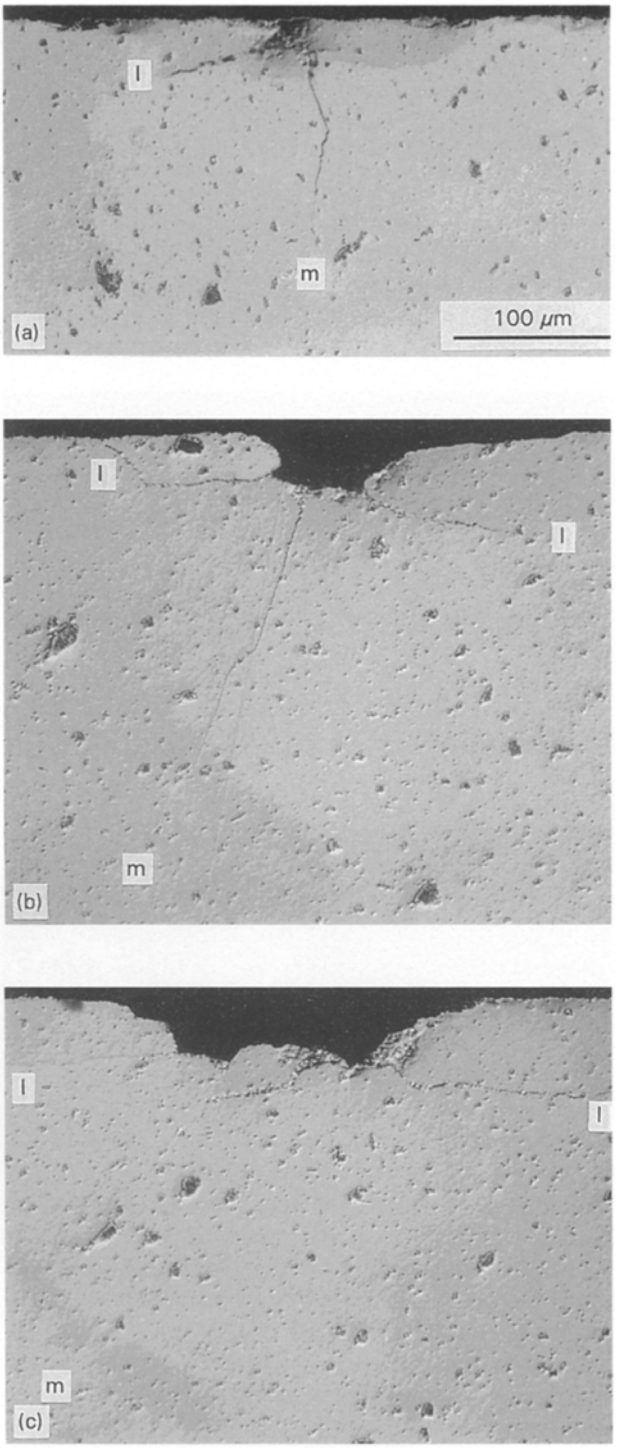

Figure 11 Optical micrographs showing subsurface scratch damage in the fine grain alumina, at $P = 40$ N after different passes: (a) $n = 1$, (b) $n = 5$ and (c) $n = 10$; "l" and "m" denote lateral and median cracks, respectively.

expanded in the form

$$\Psi(\beta l)^{1/2}\sigma_T + \Psi(\beta l)^{1/2}\sigma_D = T \qquad (4)$$

where Ψ is a crack geometry coefficient ($\Psi = 2/\pi^{1/2}$ for penny-shaped flaws).

It may be assumed that the damage-stress σ_D accumulates uniformly with time [30, 33] or with the number of passes n. Therefore, $\sigma_D = \dot{\sigma}_D n$, where $\dot{\sigma}_D$ is the damage-stress accumulation rate. Formation of damage, however, must be related to the local tensile stress σ_T due to the applied load, provided that the magnitude of the local stress is larger than a threshold value necessary for damage formation. Therefore, it is assumed that $\dot{\sigma}_D = \alpha\sigma_T^m$, where α and m are material dependent constants. Equation 4 can be rewritten as

$$\Psi(\beta l)^{1/2}\sigma_T(1 + \alpha n_c\sigma_T^{m-1}) = T \qquad (5)$$

This condition is satisfied when the number of passes reaches a critical value, i.e., $n = n_c$. As the number of passes continues to increase at $n > n_c$, additional grain facets satisfy the microcracking criterion and the number of microcracked grain boundary facets increases. According to Liu and Fine [30] and based on the fracture criterion of Fu and Evans [32], the fraction f of microcracked facets within the stressed region can be found from the fracture criterion of Equation 5,

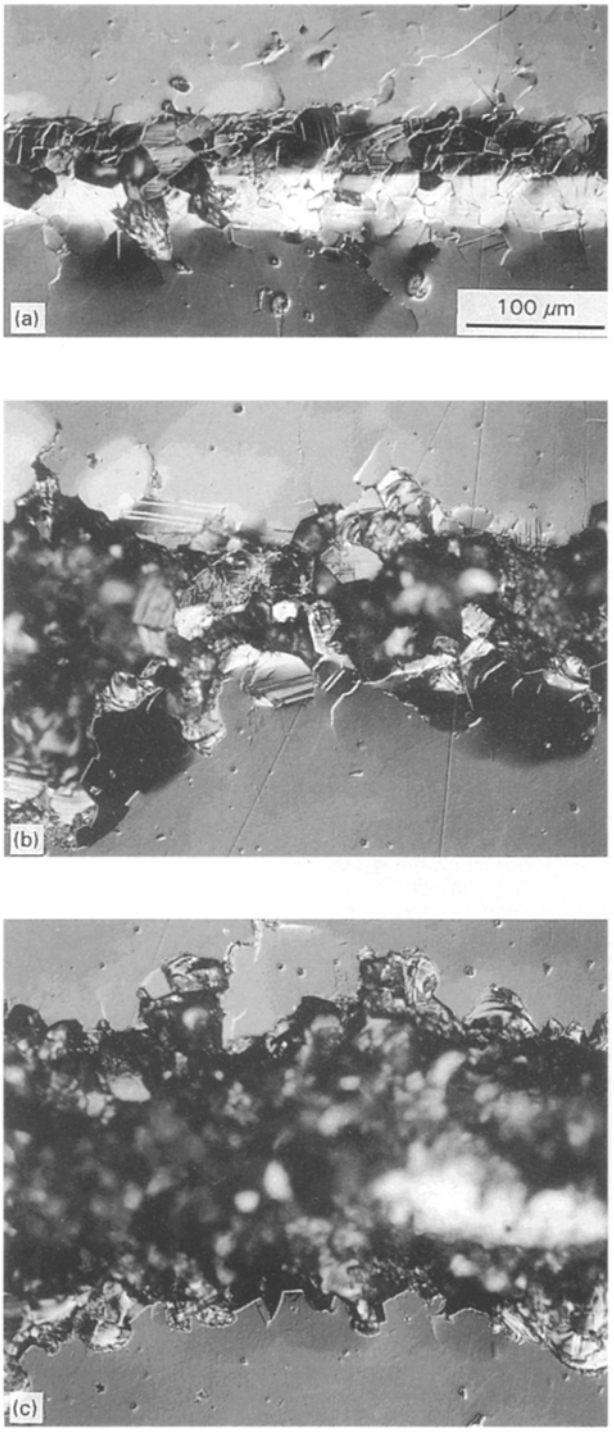

Figure 12 Optical micrographs showing the scratches produced in the coarse grain alumina at $P = 40$ N after different passes; (a) $n = 1$, (b) $n = 2$ and (c) $n = 5$.

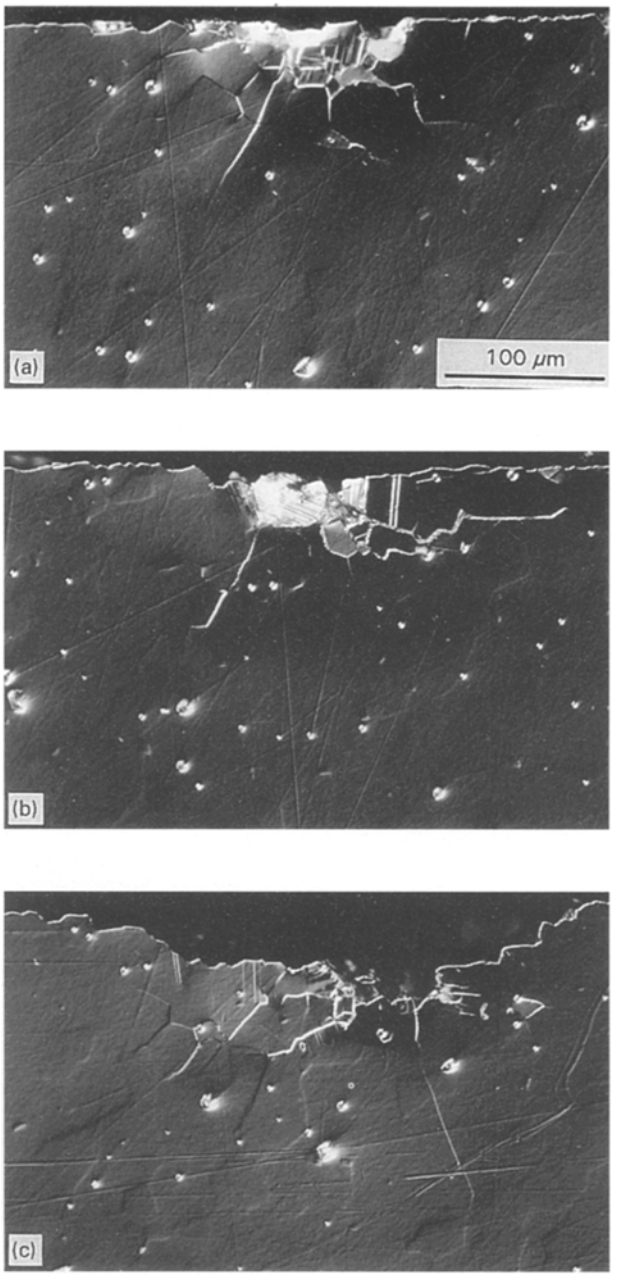

Figure 13 Optical micrographs showing subsurface damage in the coarse grain alumina at $P = 40$ N after different passes: (a) $n = 1$, (b) $n = 2$ and (c) $n = 5$. Note twin/slip bands and zigzag microcracks.

i.e.

$$f \sim \Psi(\beta l)^{1/2}\sigma_T(1 + \alpha n\sigma_T^{m-1}) - T \qquad (6)$$

for $n > n_c$.

Having established a microfracture criterion and the fraction of microcracked grain boundary facets, we now can derive an equation for the volume of removed material. Since grain dislodgement occurs within the stressed region, and particularly inside the plastic deformation zone, it is assumed that the volume of material W removed by scratching is proportional to the fraction of microcracked facets, or

$$W \sim fV_D \qquad (7)$$

where V_D is the volume of plastic zone in scratching. It has been shown [9] that the radius b of the plastic zone in indentation is related to the load P, the elastic modulus E, and the hardness H, through the following relation

$$b \sim (P/H)^{1/2}(E/H)^{2/5} \qquad (8)$$

Therefore, if L is the total scratch length, then V_D is proportional to $b^2 L$, or

$$V_D \sim (E^{4/5}/H^{9/5})PL \qquad (9)$$

The volume of material removed per unit scratch length, $V = W/L$, resulting from grain dislodgement

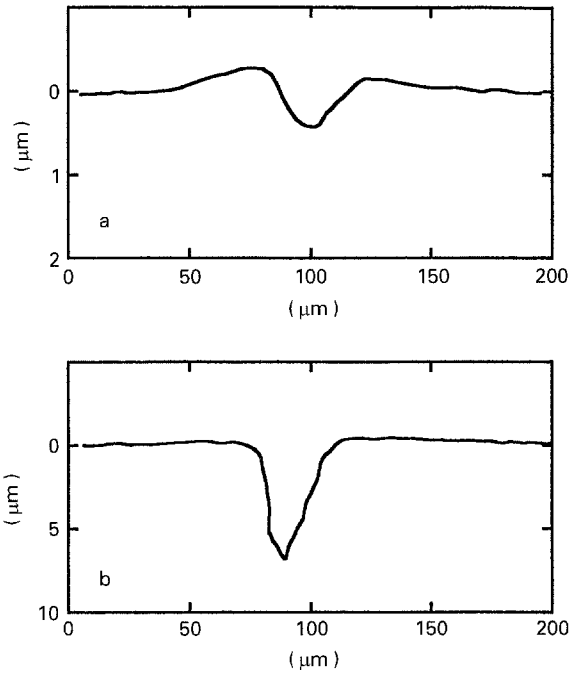

Figure 14 Profiles of the scratches made in the fine grain alumina at $P = 20$ N after (a) $n = 1$ and (b) $n = 10$. Note the raised material at the edges of the scratch in (a).

becomes

$$V = \gamma[\Psi(\beta l)^{1/2}\sigma_T(1 + \alpha n\sigma_T^{m-1}) - T](E^{4/5}/H^{9/5})P \quad (10)$$

where γ is a coefficient independent of grain size and load.

The local tensile stress σ_T is related to the applied load P [34], such that $\sigma_T \sim P^q$, where $0 \leqslant q \leqslant 1$. For example, $q = 0$ for a sharp indentor, $q = 1/3$ for Hertzian contacts, and $q = 1$ for concentrated normal force [34]. Since the scratching experiments were performed with a conical indentor with a spherical end, we set $q = 1/3$ and recast Equation 10 to the following form

$$V = (E^{4/5}/H^{9/5})[A_D(P^{4/3} + \alpha nP^{(1+m/3)}l^{1/2} - A_T TP] \quad (11)$$

where A_D and A_T are constants.

Equation 11 directly relates the volume of removed material to the applied load P, grain size l, elastic modulus E, hardness H and short-crack toughness T. This equation shows that the microfracture-controlled material removal process is enhanced by increasing the grain size, load and the Young's modulus, and it is inhibited by increasing the hardness and toughness of the material. It should be recognized that the toughness in Equation 11 is not the intrinsic grain boundary toughness T_0 (related to the surface energy), nor the long-crack toughness K_c (measured by conventional techniques using notched specimens), but the *short-crack* toughness corresponding to small initial flaws on the order of grain size. This short-crack toughness $T(\beta l)$ is increased by increasing T_0, but decreased by increasing the intrinsic thermal residual stress σ_I, as is obvious in Equation 3.

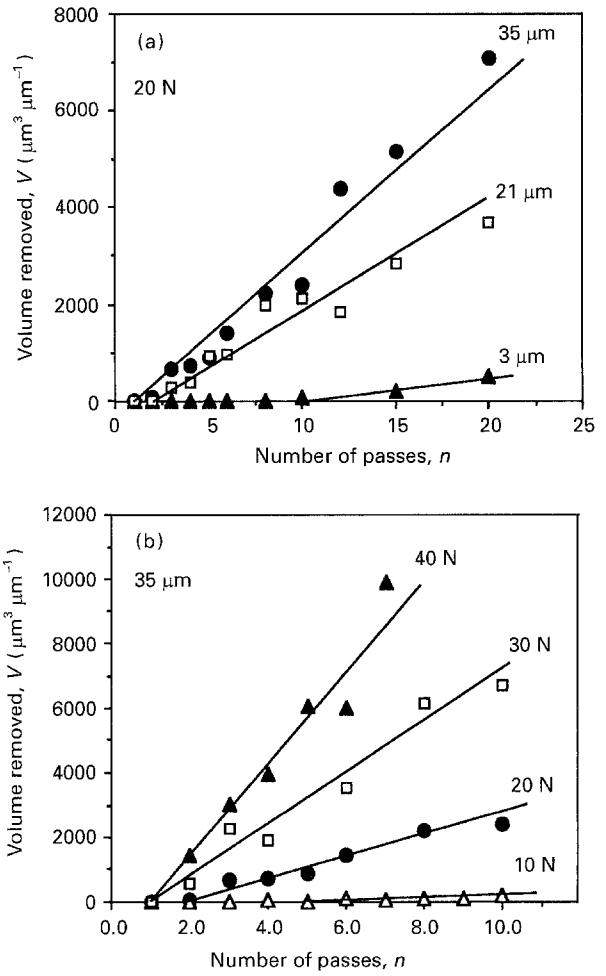

Figure 15 Volume removed per unit scratch length as a function of number of passes: (a) for three different grain sizes at $P = 20$ N (● 35 μm; □ 21 μm; ▲ 3 μm) and (b) at different loads for the coarse grain alumina (35 μm) (▲ 40 N; □ 30 N; ● 20 N; △ 10 N).

Equation 11 can be used to calculate the critical number of passes required for initiation of microfracture. This is simply accomplished by setting Equation 11 to zero, i.e. $V = 0$, which is the same as just satisfying the fracture criterion in Equation 5. The following relationship can be found for n_c

$$n_c = [(A_T/A_D)Tl^{-1/2}P^{-1/3} - 1]/(\alpha P^{(m-1)/3}) \quad (12)$$

This equation indicates that n_c is inversely related to the square root of grain size and to the load for $m > 0$.

The proposed model can be evaluated using the experimental data obtained in scratching. Equation 11 predicts that the material removal rate dV/dn in units of $\mu m^3 \mu m^{-1} pass^{-1}$, or $\mu m^2 pass^{-1}$, is proportional to $P^{(1+m/3)}l^{1/2}$. The experimental results shown in Fig. 15 can be used to obtain an estimate for m. First, the material removal rates are calculated from the slopes of the linear best fits to the data shown in Fig. 15. The experimental results for the material removal rates were plotted against $P^{(1+m/3)}l^{1/2}$ for different values of m. A best linear fit was found for $m \approx 3$, as shown in Fig. 16. Substituting this value for m in Equation 11 results in a load dependence for dV/dn as P^2

$$dV/dn = (E^{4/5}/H^{9/5})A_D\alpha P^2 l^{1/2} \quad (13)$$

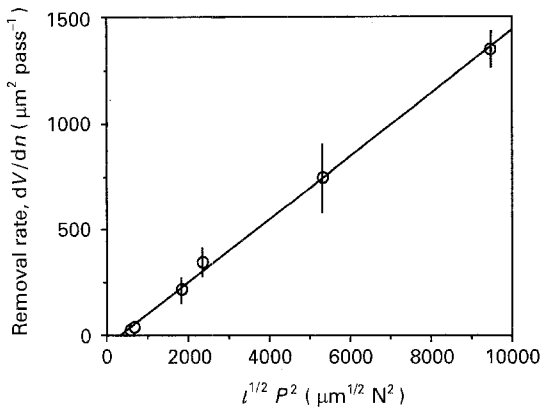

Figure 16 Material removal rates obtained from the slopes of linear best fits to the data in Fig. 15 plotted as a function of $l^{1/2}\ P^2$.

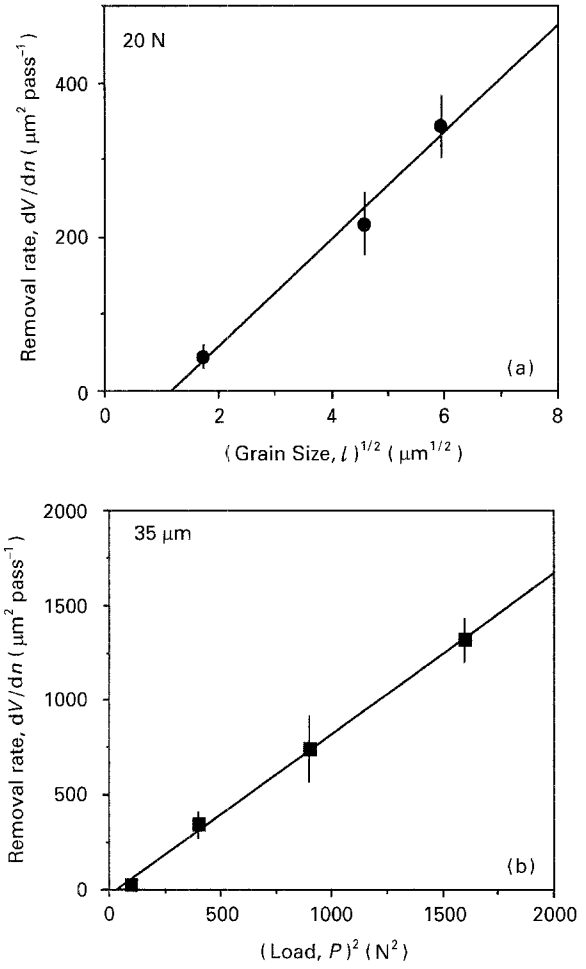

Figure 17 (a) Material removal rates obtained from the slopes of linear best fits to the data in Fig. 15(a) plotted as a function of grain size $l^{1/2}$ at load 20 N and (b) removal rate obtained from slopes of linear best fits to the data in Fig. 15(b) plotted as a function of load P^2, grain size 35 μm.

The experimental values for the removal rates are plotted in Fig. 17(a) as a function of grain size $l^{1/2}$, and in Fig. 17(b) as a function of P^2, confirming the dependence of removal rate on grain size and load.

It is noted that the three constants A_D, A_T, and α in Equations 11–13 may depend on experimental conditions including the relative humidity (or lubrication condition at the interface) and sliding speed. Also, the shape of the indentor and its mechanical properties (hardness and elastic modulus), surface roughness (roughness heights and slopes, and asperity density) are expected to influence the value of these constants. These constants can be calculated by using the experimental data and Equations 11–13. It is of particular interest to calculate α since its value can provide an insight into the relative importance of K_T and K_D in Equation 2, or the contributions of the local tensile stress σ_T due to the applied stress with respect to the tensile stress σ_D due to damage accumulation (see Equations 4 and 5). The value of α is determined by using Equation 12 and the experimentally obtained data for n_c by setting $m = 3$. It can be shown that α is inversely related to the applied load. For $P \leqslant 1\ N$, the contribution of the local tensile stress σ_T due to the applied stress to the fracture process becomes comparable to or larger than the contribution of the damage-stress σ_D. At high loads, however, the contribution of σ_D becomes overwhelming. In this case, which is applicable to our experiments on alumina, the relative contribution of σ_T to the material removal process can be ignored, and the equations for the removed volume and the critical number of passes for initiation of fracture can be simplified.

5. Discussion

In this study we have used repeated scratching to investigate the nature of subsurface damage and the mechanisms of material removal in alumina as a function of grain size, load, and number of passes. In the fine grain alumina, subsurface damage consisted of median and lateral cracks, as well as microcracks along the grain boundaries and intragrain twin/slip bands within the plastic zone. The nature of subsurface damage in the coarse grain alumina was found to be different from that observed in the fine grain counterpart. In this material, damage consisted primarily of twin/slip bands and intergranular microcracks, with no evidence for well-defined median and lateral cracks.

Observations of subsurface damage in these materials was made possible by the bonded-interface sectioning technique developed by Guiberteau *et al.* [22]. Conventional sectioning techniques involving post-test cutting and polishing, while providing useful information, remove the evidence for twin/slip bands and may remove some of the grains in the microcracked region [35]. The surface and subsurface damage patterns revealed by the bonded-interface sectioning technique provide key information on the mechanisms of material removal in scratching, which could be used as a simulation for abrasive wear and grinding.

Intergranular microcracking and grain dislodgement, as a mechanism of material removal, has been observed in several studies [2, 15, 36–40]. In an early work by Swain [2], SEM micrographs of scratch damage in an alumina clearly showed intergranular microcracking and grain dislodgement. In a wear study by Wu *et al.* [15], SEM micrographs of worn surfaces of relatively coarse grain alumina, zirconia,

and magnesia also indicated material removal by grain dislodgement. The same mechanism was shown to be operative in the scratch studies by Ajayi and Ludema [36, 37], who found that the lateral-cracking model failed to correlate with experimental results. Recent wear studies in alumina have shown that wear is initially controlled by plastic deformation and/or tribochemical reaction between alumina and moisture in the environment [38, 39]. However, after a critical load or a critical sliding distance was reached, the mechanism of material removal changed to one dominated by intergranular microfracture and grain dislodgement [38–40]. This transition is similar to the transition in the material removal process observed in the present study, namely a transition from deformation-controlled to microfracture-controlled process.

The surface and subsurface damage patterns observed in this study suggest that during scratching of alumina, material is removed by grain dislodgement resulting from intergranular microcracking. Although well-defined lateral cracks were found in the fine grain alumina, the contribution of this crack system to the material removal process was only evident when scratching was performed at large loads and after several repeated passes. This observation suggests that material removal by lateral crack chipping could become a dominant process in grinding of fine grain ceramics only if the load per grit is very large. This can occur if grinding has not been performed under an optimized condition.

Presence of machining-induced median cracks has been confirmed by fractography [41–46], where the location and source of flaws from which fracture was initiated were determined. Many examples have been reported in the literature, where fracture was first initiated from machining induced flaws, particularly the median cracks [41]. As discussed by Rice and Mecholsky [41], median cracks can reduce the strength of machined ceramics if these cracks are suitably oriented with respect to the direction of the major tensile stress in fracture testing. This suggestion has been confirmed by four-point flexure tests. It has been observed that the fracture strength of ceramic bars ground in the longitudinal direction is relatively insensitive to the grinding condition [42, 43]; whereas the strength is reduced if grinding is performed in the transverse direction [44, 45]. Rice [45] has recently shown that the extent of reduction in strength as a result of transverse grinding is related to the grain size. In alumina, a large reduction in strength was observed at a grain size of 0.7 μm; whereas the strength of the alumina with a grain size of 30 μm was only slightly reduced by grinding in the transverse direction [45]. This result is consistent with our observations that strength-reducing median cracks only form in fine grain aluminas. Presence of median cracks, however, cannot be used as an indication that in grinding material is removed by the extension of lateral cracks. In our experiments we have shown that although the median and lateral cracks may be present (especially in fine grain aluminas), material is still removed by grain dislodgement.

6. Conclusions

1. The bonded-interface sectioning technique and subsequent observations using optical microscopy with Nomarski interference illumination and SEM were demonstrated to be effective in revealing the mode of subsurface damage in scratching of alumina ceramics.

2. In the fine grain alumina, the lateral and median crack system was observed, together with intergranular microcracks and intragrain twin/slip bands distributed within the plastic zone. The distributed form of damage, namely twin/slip bands and intergranular microcracks, were also observed in the coarse grain alumina; but no evidence was found for the median and lateral cracks in this material.

3. For the three aluminas (grain size $l = 3$, 21 and 35 μm) tested under normal scratching loads of 10, 20, 30 and 40 N, the mechanism of material removal was identified as grain dislodgement resulting from grain boundary microcracking. Extension of lateral cracks contributed to the material removal process only for the fine grain alumina after several passes under a large contact load.

4. A model for the microfracture-controlled material removal process was developed that relates the volume of material removed to the applied load and material properties including grain size, elastic modulus, hardness, and *short-crack* toughness. Removal rate was found to be proportional to grain size $l^{1/2}$ and to load P^2.

Acknowledgements

The authors gratefully thank B. R. Lawn for encouragement and fruitful discussions and P. Chantikul and S. J. Bennison for providing the alumina specimens. Thanks are also due to L. Smith for providing the diamond indentor and L. K. Ives for assistance with SEM examinations. This research was sponsored in part by the Advanced Research Project Agency – Ceramic Program and the US Navy – Man Tech Program administered by the Advanced Manufacturing Research Facility at NIST.

References

1. B. R. LAWN and R. WILSHAW, *J. Mater. Sci.* **10** (1975) 1049.
2. M. V. SWAIN, *Proc. R. Soc. Lond. A.* **366** (1979) 575.
3. H. P. KIRCHNER, R. M. GRUVER and D. M. RICHARD, in "The science of ceramic machining and surface finishing II", edited by B. J. Hockey and R. W. Rice, National Bureau of Standards SP 562 (Government Printing Office, Washington, DC, 1979) p. 23.
4. A. B. GROENOU, N. MAAN and J. B. D. VELDKAMP, in "The science of ceramic machining and surface finishing II", edited by B. J. Hockey and R. W. Rice, National Bureau of Standards SP 562 (Government Printing Office, Washington, DC, 1979) p. 43.
5. H. P. KIRCHNER, *J. Amer. Ceram. Soc.* **67** (1984) 127.
6. W. CHENG, E. LING and I. FINNIE, *ibid.* **73** [3] (1990) 580.
7. D. B. MARSHALL, A. G. EVANS, B. T. K. YAKUB, J. W. TIEN and G. S. KINO, *Proc. R. Soc. Lond. A.* **385** (1983) 461.
8. A. G. EVANS, in "The science of ceramic machining and surface finishing II", edited by B. J. Hockey and R. W. Rice, National Bureau of Standards SP 562 (Government Printing Office, Washington, DC, 1979) p. 1.

9. A. G. EVANS and D. B. MARSHALL, in "Fundamentals of friction and wear of materials", edited by D. A. Rigney (ASME Press, New York, 1981) p. 439.
10. S. MALKIN and J. E. RITTER, *Transactions of the ASME* **111** (1989) 167.
11. J. MUKERJI and P. K. DAS, *J. Amer. Ceram. Soc.* **76** [9] (1993) 2376.
12. R. W. RICE and B. K. SPERONELLO, *ibid.* **59** [7–8] (1976)330.
13. L. F. GOYETTE, T. J. KIM and P. J. GIELISSE, *Ceram. Bull.* **56** [11] (1977) 1018.
14. R. W. RICE and R. C. POHANKA, *J. Amer. Ceram. Soc.* **62** [11–12] (1979) 559.
15. C. CM. WU, R. W. RICE, D. JOHNSON and B. A. PLATT, *Ceram. Engrg. Sci. Proc.* **6** [7–8] (1985) 995.
16. C. CM. WU, R. W. RICE, B. A. PLATT and S. CARRLE, *ibid.* **6** [7–8] (1985) 1023.
17. R. W. RICE, *J. Amer. Ceram. Soc.* **76** [4] (1993) 1068.
18. P. CHANTIKUL, S. J. BENNISON and B. R. LAWN, *ibid.* **73** [8] (1990) 2419.
19. S. J. BENNISON and B. R. LAWN, *Acta Metall.* **37** [10] (1989) 2659.
20. D. B. MARSHALL, B. R. LAWN and R. F. COOK, *J. Amer. Ceram. Soc.* **70** [6] (1987) C-139.
21. P. ROTH and H. K. TONSHOFF, in "Machining of advanced materials", edited by S. Jahanmir, National Institute of Standards and Technology SP 847 (Government Printing Office, Washington, DC, 1993) p. 247.
22. F. GUIBERTEAU, N. P. PADTURE and B. R. LAWN, *J. Amer. Ceram. Soc.* **77** [7] (1994) 1825.
23. F. GUIBERTEAU, N. P. PADTURE, H. CAI and B. R. LAWN, *Phil. Mag.* **A68** [5] (1993) 1003.
24. H. CAI, M. A. S. KALCEFF and B. R. LAWN, *J. Mater. Res.*, **9** [3] (1994) 762.
25. N. P. PADTURE and B. R. LAWN, *J. Amer. Ceram. Soc.* **77** [10] (1994) 2518.
26. H. H. K. XU, L. WEI, N. P. PADTURE, and B. R. LAWN, *J. Mater. Sci.*, in press.
27. H. H. K. XU and S. JAHANMIR, *J. Amer. Ceram. Soc.*, **77** [5] (1994) 1388.
28. *Idem, J. Mater. Sci. Lett.*, in press.
29. D. B. MARSHALL, B. R. LAWN and A. G. EVANS, *J. Amer. Ceram. Soc.* **65** [11] (1982) 561.
30. S. J. CHO, B. J. HOCKEY, B. R. LAWN and S. J. BENNISON, *J. Amer. Ceram. Soc.* **72** [7] (1989) 1249.
31. H. LIU and M. E. FINE, *ibid.* **76** [9] (1993) 2393.
32. Y. FU and A. G. EVANS, *Acta. Metall.* **33** [8] (1985) 1515.
33. B. R. LAWN, "Fracture of brittle solids" (Cambridge University Press, Cambridge, 1993) chapters 7 and 10.
34. K. L. JOHNSON, "Contact mechanics" (Cambridge University Press, Cambridge, 1985) chapter 3.
35. B. ZHANG, H. TOKURA and M. YOSHIKAWA, *J. Mater. Sci.* **23** (1988) 3214.
36. O. O. AJAYI and K. C. LUDEMA, "Wear of Materials" (ASME, 1987) p. 349.
37. *Idem., ibid.* (ASME, 1991) p. 307.
38. X. DONG and S. JAHANMIR, *J. Amer. Ceram. Soc.* **74** [5] (1991) 1036.
39. S. JAHANMIR and X. DONG, *J. Tribology* **114** (1992) 403.
40. S. J. CHO, H. MOON, B. J. HOCKEY and S. M. HSU, *Acta Metall. Mater.* **40** [1] (1992) 185.
41. R. W. RICE and J. J. MECHOLSKY, Jr., in "The science of ceramic machining and surface finishing II", edited by B. J. Hockey and R. W. Rice, National Bureau of Standards SP 562 (Government Printing Office, Washington, DC, 1979) p. 351.
42. S. JAHANMIR, T. J. STRAKNA, G. D. QUINN, H. LIANG, R. L. ALLOR and R. D. WEST, in "Machining of advanced materials", edited by S. Jahanmir, National Institute of Standards and Technology SP 847 (Government Printing Office, Washington, DC, 1993) p. 263.
43. S. JAHANMIR, T. J. STRAKNA, G. D. QUINN, R. N. KOPP, S. C. YOON and K. V. KUMAR, in "Machining of advanced materials", edited by S. Jahanmir, National Institute of Standards and Technology SP 847 (Government Printing Office, Washington, DC, 1993) p. 279.
44. T. J. STRAKNA, S. JAHANMIR, R. L. ALLOR and K. V. KUMAR, in preparation.
45. R. W. RICE, in "Machining of advanced materials", edited by S. Jahanmir, National Institute of Standards and Technology SP 847 (Government Printing Office, Washington, DC, 1993) p. 185.
46. R. W. RICE, S. W. FREIMAN, J. J. MECHOLSKY, Jr., R. RUH and Y. HARADA, in "Ceramics for high temperature applications II", edited by J. Burke, E. Lenoe and R. Katz (Chesnut Hill, MA, 1978) p. 669.

Received 29 April
and accepted 11 August 1994